Electrical and optical properties of radiation-induced dominant recombination center in $In_xGa_{1-x}P$ space solar cells

M. Adachi,[1] A. Khan,[2] K. Ando,[3] N. J. Ekins-Daukes,[4] H. S. Lee,[5] and M. Yamaguchi[5]
[1]*Venture Business Laboratory, Tottori University, Koyama, Tottori 680, Japan*
[2]*Department of Electrical and Computer Engineering, University of South Alabama, Mobile, Alabama 36688, USA*
[3]*Department of Electrical and Electronic Engineering, Tottori University, Koyama, Tottori 680, Japan*
[4]*School of Physics, University of Sydney, Sydney, New South Wales, 2006, Australia*
[5]*Toyota Technological Institute, 2-12-1 Hisakata, Tempaku, Nagoya 468-8511, Japan*
(Received 10 June 2005; revised manuscript received 18 August 2005; published 21 October 2005)

We have performed detailed studies on the stability of the major irradiation-induced defect *H*2 in *p*-$In_xGa_{1-x}P$ under various biases, in order to clarify the dependence of reaction rates on the position of the Fermi level in the absence of minority-carrier injection and electron-hole recombination. The dependence of the annealing rates on the electrical injection current has been analyzed at different temperatures by using a variety of electrical and optical experiments, such as deep-level transient spectroscopy, thermally stimulated capacitance, deep-level optical spectroscopy (DLOS), and photocapacitance (PHCAP). The energy of multiphonon emissions due to *e-h* recombination at the *H*2 center is estimated to be 1.36 eV. The capture cross section of the *H*2 trap for electrons under *e-h* recombination process is evaluated as $\sigma_n = 3 \times 10^{-12}$ cm^2, which is found to be significantly larger than the hole capture cross section ($\sigma_p = 1 \times 10^{-16}$ cm^2). The photoionization energy 0.94 ± 0.10 eV is estimated by DLOS and confirmed by PHCAP experiments. The Frank-Condon shift value is estimated to be 0.45 ± 0.10 eV. In order to fully explain the athermal annihilation mechanism of the *H*2 center under minority-carrier injection condition, a configuration coordinate diagram model has been proposed based on the measured physical parameters in this study.

DOI: 10.1103/PhysRevB.72.155320 PACS number(s): 78.66.−w, 71.55.Eq, 73.40.Kp

I. INTRODUCTION

Present in-depth physics-based studies fully explore the role of the major irradiation-induced center *H*2 in *p*-$In_xGa_{1-x}P$ as an efficient electron-hole (*e-h*) recombination center. The *e-h* recombination energy at the *H*2 center promotes the recombination-enhanced defect reaction (REDR) process under minority-carrier injection. In order to develop $In_xGa_{1-x}P$-based multijunction solar cell technology for space applications, it is crucial to understand the nature of radiation-induced defects, which affect material properties and device performance in the space environment.

Recently, we have reported the dominant role of the major radiation-induced defect (*H*2 center) in $In_xGa_{1-x}P$, and recovery of the solar cell properties under minority-carrier injection annealing.[1–4] The marked recovery of radiation damage, output power, and electron diffusion length in $In_xGa_{1-x}P$ solar cells induced by minority-carrier injection was found to correlate with the annihilation of the *H*2 defect.[1]

In addition, our previous study based on thermal deep-level transient spectroscopy (DLTS) revealed that the minority-carrier injection annealing of the *H*2 center is related to the energy release mechanism.[5] However, the full identification of the mechanism based on electrical and optical characteristics of the *H*2 center was unresolved.

The purpose of this study is to fully characterize the dominant irradiation-induced *H*2 center in *p*-$In_xGa_{1-x}P$ electrically and optically, in order to understand the mechanism involved in the minority-carrier-injection annealing kinetics. Detailed studies have been performed on the stability of the defect *H*2 under various biases, and of the dependence of the annealing rates on electrical injection current density at different temperatures, by using a variety of electrical and optical techniques such as DLTS, double-carrier DLTS (DCDLTS) (see Sec. II B), thermally stimulated capacitance (TSCAP),[6] deep-level optical spectroscopy (DLOS),[7] and photocapacitance (PHCAP).[8,9] The motivation to use these techniques is to correlate the results with different experimental approaches, and proposed a unified configuration-coordinate diagram of the *H*2 center in order to identify the recombination-enhanced defect reaction (REDR) in $In_xGa_{1-x}P$ material and solar cells.

II. EXPERIMENTAL DETAILS

A. Sample preparation

The samples studied were n^+-*p* junction $In_{0.5}Ga_{0.5}P$ diodes, grown on GaAs substrates by metal organic chemical vapor deposition. The n^+ emitter was Si doped at a level of 3×10^{18} cm^{-3} and the base (0.55 μm thick) was Zn doped at levels of $5 \times 10^{16} - 1.5 \times 10^{17}$ cm^{-3} (Fig. 1). The defects were introduced at room temperature by 1 MeV electron irradiation, using a Van de Graaff accelerator. The electron fluence ranged from 2×10^{15} to 3×10^{16} cm^{-2}, with a flux density of 1×10^{12} cm^{-2} sec^{-1}, low enough to avoid significant sample heating during irradiation. The electron beam was scanned in order to ensure a uniform irradiation over the whole surface of the sample.

B. Experimental method

Conventional current-voltage (*I-V*) and DLTS measurements were performed, coupled with capacitance-voltage

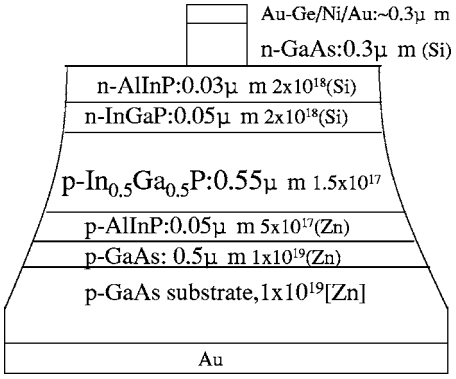

FIG. 1. A schematic diagram of the $In_xGa_{1-x}P$ space solar cell used in this study.

(*C-V*) measurements in order to determine the doping concentration in the *p*-type $In_xGa_{1-x}P$-based layer. The characteristics of the defects were then extracted from the DLTS signals. The study of the capture of a minority carrier (electron) at a majority-carrier trap (the *H*2 center) has been carried out by using the DCDLTS technique (see Sec. II B).

In order to avoid a possible thermal effect, the isothermal capacitance transient spectroscopy mode has been used for minority-carrier-injection annealing measurements.

For optical measurements, PHCAP and DLOS, the samples were illuminated with monochromatic light in the range of 600–1200 nm at low enough temperature that the thermal emission rate e^{th} from the deep level was negligibly small compared to the optical emission rate e^{opt} ($e^{th} \ll e^{opt}$). The time-dependent photocapacitance signal was measured with a capacitance meter operating at 1 MHz. The DLOS experiment was carried out with a rate window of 35 msec in the DLTS system. The change in photocapacitance in the specified time interval, were recorded as PHCAP and DLOS signals as a function of the photon energy.

C. Principle of double-carrier DLTS technique

Here we present the principle of the DCDLTS technique, which can quantify the electron-hole recombination characteristics of deep levels by using both carrier types (majority and minority carriers) controlled by double-pulse biases as shown in Fig. 2(a).

First, majority carriers are injected by the pulse at $t=0$. After a delay W_{1st} a second minority pulse of width W_{2nd} is applied, as shown in Fig. 2(a). The concentration of an ionized trap $n_T(t)$ in the *p*-type layer can be expressed using the rate equation[10] as follows:

$$dn_T(t)/dt = -e_n n_T(t) + nC_n[N_T - n_T(t)] - pC_p n_T(t) + e_p[N_T - n_T(t)];$$

therefore

$$n_T(W_{2nd}) = n_T(\infty)[1 - \exp(-\tau^{-1}W_{2nd})] + n_T(0)\exp(-\tau^{-1}W_{2nd}), \quad (1)$$

where

$$n_T(\infty) = (\langle n\rangle C_n + e_p)/(\langle n\rangle C_n + pC_p + e_n + e_p)N_T,$$

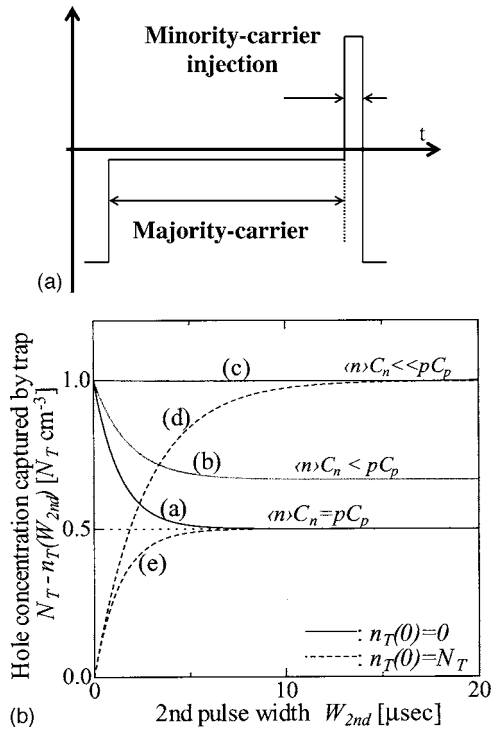

FIG. 2. (a) Double-pulse bias profile in the DCDLTS experiment. V_{1st} and V_{2nd} control majority- and minority-carrier injection, respectively. (b) Simulation of occupation probability of majority-carrier (hole) for a deep-level trap under minority-carrier injection. The parameters used in this simulation are for curves *a* and *e*, $n=p=1\times10^{16}$ cm^{-3}, $C_n=C_p=\langle v_{th(n)}\rangle\sigma_n=\langle v_{th(p)}\rangle\sigma_p=10^5-10^{-22}$ m^3/sec, $e_n=e_p=1000$ sec^{-1}; curve *b*, same conditions as *a* except for $\langle n\rangle=5\times10^{15}$ cm^{-3}; curves *c* and *d*, also the same as *a* except for $\langle n\rangle=0$.

$n_T(t)$ and N_T are the concentrations of ionized traps and defect concentrations, e_p and e_n are emission rate for holes and electrons, C_p and C_n are the capture rates for holes and electrons ($=\langle v_{th(p)}\rangle\sigma_p$ and $\langle v_{th(n)}\rangle\sigma_n$), $\langle v_{th(p)}\rangle$ and $\langle v_{th(n)}\rangle$ are the thermal velocities for the holes and electrons, σ_p and σ_n are capture cross section for the hole and electron, respectively, $\langle n\rangle$ is the averaged concentration of injected minority carriers, and p is the free hole concentration in the *p*-type layer.

Based on Eq. (1), we can simulate the occupation probability of majority carriers (holes) for a deep-level trap under minority-carrier injection as shown in Fig. 2(b). After minority-carrier injection, one can see that the hole concentration captured by the trap decreases with increasing minority-carrier capture rate $\langle n\rangle C_n$.

In order to conveniently evaluate the characteristics of a deep level, we simply express Eq. (1) as follows:

$$n_T(W_{2nd})/N_T = \{S_{DLTS} - S_{DCDLTS}\}/\{S_{DLTS}\} = \langle n\rangle\sigma_n\langle v_n\rangle W_{2nd}, \quad (2)$$

where S_{DLTS} and S_{DCDLTS} are the DLTS and DCDLTS signal intensities, respectively. Equation (2) is obtained from the following conditions:

$$n_T(0) = 0 \ (W_{1st} \gg 1/pC_p),$$

$$e_n \quad \text{and} \quad e_p \ll \langle n \rangle C_n \quad \text{and} \quad pC_p,$$

$$\langle n \rangle C_n \gg pC_p \quad \text{and} \quad 1 \gg \langle n \rangle C_p W_{2nd},$$

which can be satisfied by appropriate majority- and minority-carrier injection conditions, W_{1st}, W_{2nd}, and $\langle n \rangle$.

Therefore, evaluating the DLTS signal intensity after minority-carrier injection, i.e., the DCDLTS signal intensity, one can determine the *e-h* recombination characteristics such as the minority-carrier-capture cross section σ_n under the *e-h* recombination process, *e-h* recombination barrier height, and *e-h* recombination rate of a deep-level trap.

In this paper the analysis assumed the following physical parameters for the $In_xGa_{1-x}P$ diode: $m_n^*=0.21$, $m_p^*=0.80$, $\varepsilon_s=11.8$, $\mu_n=1000$ cm^2/V sec at 300 K (and the temperature dependency $\mu_n \propto T^2$), and $\mu_p=120$ cm^2/V sec at 300 K ($\mu_p \propto T^2$). The parameter giving the largest error to the analysis was the minority-carrier lifetime τ_n in the *p*-type layer. It is estimated at 0.1 nsec based on our basic electron beam induced current (EBIC) experiment, and $\tau_p=1$ nsec in the *n*-type layer.

III. RESULTS AND DISCUSSION

A. Various annealing properties on the *H*2 center

In order to clarify the mechanism involved in minority-carrier injection-enhanced annealing of the radiation-induced defects in *p*-$In_xGa_{1-x}P$, we have performed a detailed study of the stability of the defects under reverse-bias and zero-bias conditions, and of the dependence of the annealing rates on the injection current density at different temperatures.

We carried out a systematic study of the variation of the concentration of the deep-level *H*2 using a constant forward-bias injection (0.1 A/cm^2) at various temperatures for 0.5, 1, 2, 5, 10, and 20 min. We observed very interesting changes in the strength of the peak *H*2 in our DLTS signal following forward-bias minority-carrier injection.[1]

The annealing rates of the *H*2 trap in *p*-$In_xGa_{1-x}P$ under zero-bias, reverse-bias and forward-bias conditions have been measured as a function of temperature by recording the DLTS signal after each annealing step. Figure 3 compares the Arrhenius plots of the annealing rates versus inverse temperature under the various bias conditions. Interestingly, there is no difference between reverse-bias and zero-bias conditions, i.e., when the defect state is free of holes (under an applied reverse bias) and filled by holes (at zero bias). This observation rules out a charge state effect as being responsible for the annihilation of the *H*2 center under minority-carrier injection. Furthermore, it is very interesting to note that minority-carrier injection causes a substantial reduction in the annealing activation energy E_J, 0.51 eV as compared to the thermal annealing E_{th} of 1.68 eV (Fig. 4).

Here we discuss the defect reaction mechanism based on the experimental results. In order to explain the recombination-enhanced mechanisms[11–21] in III-V semiconductors, two basic mechanisms have been proposed: the so-called energy release mechanism and the Bourgoin mechanism.[18,19] According to these mechanisms, defect migration energy, equilibrium, and saddle-point configurations can be charge state dependent because of the electron-phonon interaction of the defect with the host atoms. As a result, trapping of a carrier, or successive trapping of carriers of opposite charge, can result in the enhancement of defect migration. Similarly, a change of charge states due to capture of carriers can result in electron-phonon coupling. That is, vibration relaxation takes place, which may activate various reactions of the defect such as its migration and destruction, resulting ultimately in the generation of heat in the lattice.

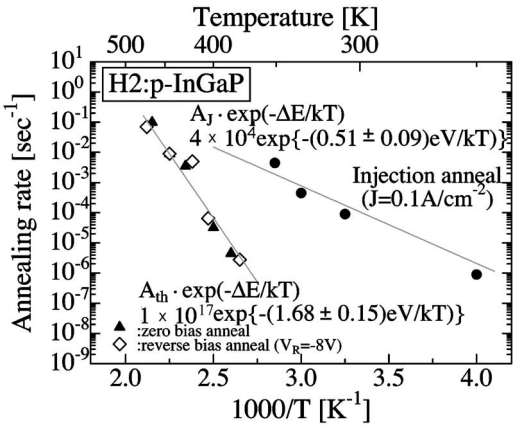

FIG. 3. The annealing rates of the *H*2 center under pure-thermal, reverse-bias, and minority-carrier injection conditions vs $1/T$. Annealing kinetics for the *H*2 deep trap in *p*-$In_xGa_{1-x}P$ are determined by DLTS experiments under the conditions of reverse, zero, and forward biases (0.1 A/cm^2).

We now consider the *e-h* recombination energy at the localized *H*2 trap, based on its athermal rate. The temperature dependence of the annealing rate of the *H*2 center under

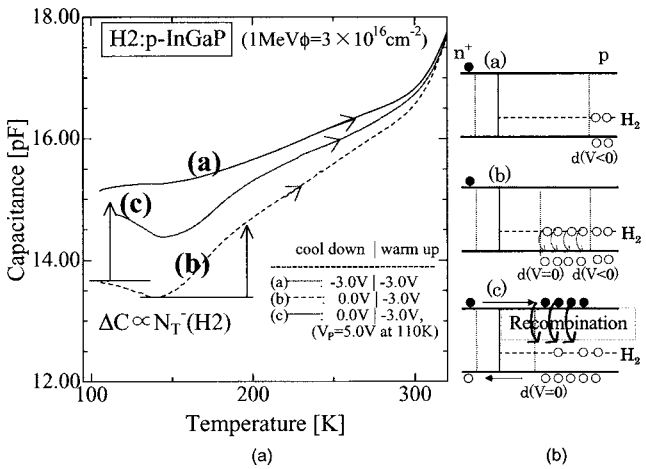

FIG. 4. (a) TSCAP signal when (curve *a*) cooling with reverse bias; (curve *b*) cooling with applied zero bias to allow trap filling; at 110 K a reverse bias is applied; and (curve *c*) cooling with applied zero bias and rewarming with applied reverse bias after minority-carrier injection at 110 K. (b) The hole occupation probability for the *H*2 trap from TSCAP experiments. *a*, *b*, and *c* correspond to the curves *a*, *b*, and *c* in (a), respectively.

minority-carrier injection condition can be expressed as

$$R^*(T) = (4 \times 10^4 \text{ sec}^{-1})\exp[-(0.51 \pm 0.09 \text{ eV})/kT], \quad (3)$$

which can be compared to following equation proposed by Kimerling *et al.*:

$$R^*(T) = A^* \exp[-(\Delta H^{th} - E^{rec}_{e\text{-}h})/kT], \quad (4)$$

where, A^* is the prefactor of the reaction rate, ΔH^{th} is the activation energy under a pure thermal annealing process, $E^{rec}_{e\text{-}h}$ is the *e-h* recombination energy at the trap, and k is the Boltzmann constant. Compared to the experiments, they can be estimated at $A^*=4\times10^4$ sec^{-1}, $\Delta H^{th}=1.68\pm0.15$ eV and $E^{rec}_{e\text{-}h}$ is 1.17 ± 0.17 eV. The part of the exponent of the reaction rate $\Delta H^{th}-E^{\text{rec}}_{e\text{-}h}$ (energy barrier) gives the activation energy under minority-carrier injection, and the electronic energy ($E^{rec}_{e\text{-}h}\approx1.2$ eV) which contributes to the defect reaction rate is the *e-h* nonradiative recombination energy at the localized *H*2 center.

The above discussion is, however, based on some assumptions, that the dominant irradiation-induced *H*2 center in $In_xGa_{1-x}P$ acts as an efficient nonradiative *e-h* recombination center, and the recombination energy is transferred to the defect reaction process. The following should therefore be verified: (i) the nonradiative *e-h* recombination characteristics of the trap; (ii) the temperature-dependent capture cross section, in order to verify multiphonon emission; (iii) the optical ionization energy of the trap for holes, in order to evaluate the Frank-Condon shift, which corresponds to the electron-lattice interaction (lattice relaxation) energy.

Thus we carried out experiments to determine the above physical parameters of the dominant irradiation-induced *H*2 center in $In_xGa_{1-x}P$-based solar cells.

B. Nonradiative *e-h* recombination characteristics on the *H*2 center

1. Verification of nonradiative e-h recombination center on the H2 center

a. Thermally stimulated capacitance analysis. First, in order to verify the *e-h* recombination at the *H*2 center qualitatively, a thermally stimulated capacitance measurement was performed. The curves shown in Fig. 4(a) give the change in capacitance for an electron-irradiated cell as a function of temperature, as the sample is heated from 110 K. The curves *a*, *b*, and *c* in Fig. 4(a) correspond to the following bias conditions.

(i) Cooling from room temperature to 110 K under reverse bias and followed by warming with no change in bias. This curve (*a*) corresponds to the temperature dependent capacitance of the sample in the absence of carrier emission since no capture was allowed. This image is shown in Fig. 4(b) curve *a*. The *H*2 trap was not filled with holes during the scanning of the temperature. This provides the reference curve marked *a* in Fig. 4(a).

(ii) Sample is cooled from room temperature to 110 K under zero applied bias to allow trap filling at the *H*2 center. At 110 K, a reverse bias is applied during the TSCAP heating scan. The hole emission process from *H*2 is shown by curve *b* in Fig. 4(a).

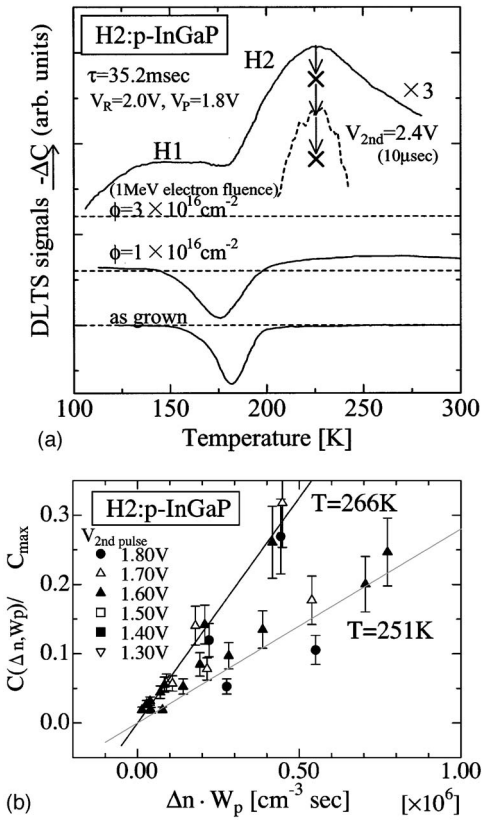

FIG. 5. (a) Systematic reduction of the DCDLTS signal intensities for the *H*2 trap under minority-carrier injection. The signal reduction indicates that the *H*2 center plays a role as an electron-hole recombination center. (b) The reduction in the DCDLTS intensities is proportional to the minority-carrier injection density $\langle n\rangle$, and to the injection pulse width W_{2nd}. Clearly, the DLTS signal intensity is decreasing systematically with increasing minority-carrier injection density $\langle n\rangle W_{2nd}$.

(iii) This condition was the same as the condition (ii) except forward bias was applied for minority-carrier injection at 110 K, in order to ionize the trap through *e-h* recombination. This condition corresponds to curve *c* in Fig. 4(a).

It is clear from Fig. 4(a) that curves *a* and *b* do not coincide at lower temperature (110–200 K), having a separation that corresponds to the change in capacitance due to the capture of a hole at the *H*2 center. The shoulder on signal *b* at about 150 K originates from the ionization of the emission of the hole for the *H*2 trap due to its activation energy (0.55 eV). The ionization due to electron injection at 110 K indicates that electron-hole recombination took place at the *H*2 center. We can see that at about 150 K, signal *c* shows a reduction of ionization from the *H*2 trap; this result also indicates that *e-h* recombination occurred at the *H*2 center at 110 K.

b. DCDLTS analysis. In order to quantify the *e-h* recombination characteristics of the *H*2 center, we carried out DCDLTS experiments.

Figure 5(a) shows DCDLTS and DLTS signals from the *H*2 trap in $In_xGa_{1-x}P$. The DLTS signals before and after 1 MeV irradiation are shown in the same figure. The *H*2 trap cannot be detected as a native defect in the sample before

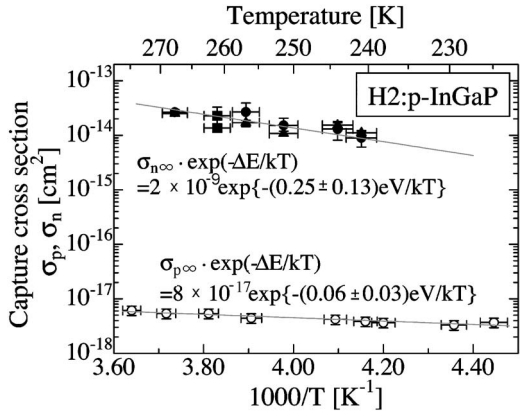

FIG. 6. The temperature dependence of the hole and electron capture cross sections of the $H2$ trap. Solid lines show a least-squares fit to the data.

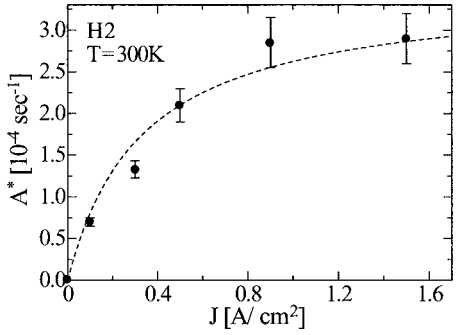

FIG. 7. Variation of the annealing rate at 300 K as a function of minority-carrier injection current density.

irradiation; however, the center shows a steady increase with increasing electron fluence.

The broken line in Fig. 5(a) shows a pronounced decrease in the $H2$ signal under the second pulse $V_{2nd}=2.4$ V, $W_{2nd}=10$ μsec.

Clearly, the DCDLTS signal intensity is decreasing systematically with increasing minority-carrier injection $\langle n\rangle W_{2nd}$. This indicates that the deep-level trap $H2$ is efficient in capturing electrons and acts as an e-h recombination center.

The reduction of the DCDLTS intensities is plotted as a function of the minority-carrier injection $\langle n\rangle W_{2nd}$ as shown in Fig. 5(b). The intensities are proportional to minority-carrier injection density $\langle n\rangle$, and to the injection pulse width W_{2nd}. Based on Eq. (2), the slope of the line in Fig. 5(b) divided by the thermal velocity of electron $\langle v_{th(n)}\rangle$ gives the capture cross section for the minority carrier, σ_n, at each temperature.

2. Measurement of capture cross section and recombination rate of the H2 center

The temperature dependence of the capture cross section was investigated by repeating the DLTS measurement, over the temperature range 220–280 K, the data are plotted in Fig. 6. One can see that the capture cross section for an electron is about three orders of magnitude greater than that of the hole at 270 K. This indicates that the $H2$ center can act as a strong electron-hole recombination center.

The capture cross sections for holes σ_p and for electrons σ_n show an increase with temperature following an Arrhenius behavior,

$$\sigma_n(T) = \sigma_n(\infty)\exp(-E_{e,cap}/kT) = (3 \times 10^{-12}\ \text{cm}^2)\exp[-(0.15 \pm 0.10\ \text{eV})/kT], \quad (5)$$

$$\sigma_p(T) = \sigma_p(\infty)\exp(-E_{h,cap}/kT) = (1 \times 10^{-16}\ \text{cm}^2)\exp[-(0.06 \pm 0.03\ \text{eV})/kT]. \quad (6)$$

$E_{e,cap}$ corresponds to the energy barrier height of the e-h recombination process. It is noteworthy that the barrier height $E_{e,cap}$ is large, indicating that at room temperature the $H2$ trap acts as an active e-h recombination center. However, at low temperature (<100 K) the center no longer acts as an e-h recombination center, owing to its large barrier height $E_{e,cap}$.

Equations (5) and (6) can be understood more clearly when compared with minority-carrier injection dependence of the annealing rates of the $H2$ trap, shown in Fig. 7. Based on the capture cross sections determined by the DCDLTS experiment, both capture rates for electron and hole at 300 K are expected to be equal at a current $J \cong 1$ A/cm^2, because the e-h recombination rate $\langle n\rangle\langle v_{th(n)}\rangle\sigma_n \cong p\langle v_{th(p)}\rangle\sigma_p = 10^5$ sec^{-1}. In the annealing experiment in Fig. 7, one can see the saturation of the annealing rate takes place about $J \cong 1$ A/cm^2. In the low-forward-current-density region in Fig. 7, the injection annealing rate A^* of the $H2$ trap is proportional to the forward current density J, because in this case the minority carrier is the limiting process such that $\langle n\rangle C_n \ll pC_p$. On the other hand, at relatively high current density (>0.8 A/cm^2) the annealing rate versus forward current density is almost close to saturation so in this case majority capture is the limiting process $\langle n\rangle C_n \gg pC_p$, with the result that the recombination rate A^* is independent of the current density.

We can confirm, therefore, that the cross sections evaluated by this study are in good agreement with the annihilation rate and the e-h recombination rate.

Further information obtained from this experiment is that the barrier heights $E_{e,cap}$,$E_{h,cap}$ are not equal to zero. This indicates that the $H2$ center should be configured when the trap captures an electron or a hole (see Sec. III D), i.e., this center is a lattice-relaxation-type defect.

From these results, it follows that (i) the $H2$ center in p-$In_xGa_{1-x}P$ acts not only as a hole trap, but also as an efficient nonradiative recombination defect under minority-carrier injection condition, e.g., the device operation condition; (ii) the driving force of the $H2$ trap under the athermal annealing process is due to the multiphonon emission induced by the e-h nonradiative recombination energy into the localized center.

In the next section we described the ionization characteristics at the $H2$ center, in order to discuss the lattice relaxation energy of the trap.

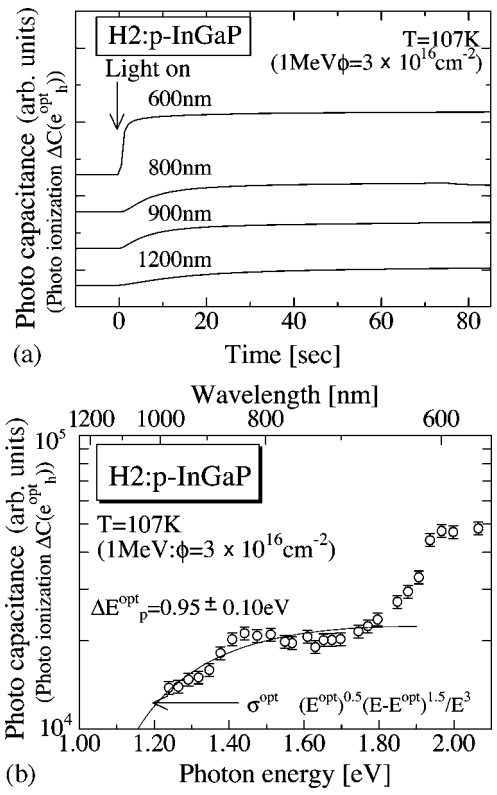

FIG. 8. (a) Photocapacitance signals for hole emission from the $H2$ trap for different photon energies. Clearly, the time constant for the ionization of the $H2$ trap depends on excitation wavelength. (b) Photocapacitance spectrum obtained at $T=107$ K as a function of photon energy. The solid curve in the figure is a theoretical curve (Ref. 12). The threshold photoionization energy was estimated at 0.95 ± 0.10 eV by theoretical fitting.

C. Optical ionization characteristics at the *H*2 center

1. Photocapacitance analysis

To further elucidate the role of the $H2$ trap as a lattice-relaxation-type defect, we measured the optical characteristics of the $H2$ center using photocapacitance analysis. This method uses optical excitation to monitor deep levels in a semiconductor, and the data take the form of the spectrum of the steady-state capacitance as a function of photon energy.

For the measurements of PHCAP and DLOS, the sample was first applied with zero bias followed by reverse bias -3 V, in order to fill the $H2$ center with holes. After applying the reverse bias, the change in the capacitance was monitored under illumination with monochromatic light in the range of $600-1200$ nm at sufficiently low temperature ($e^{th} \ll e^{opt}$). Then the time-dependent photocapacitance signals were measured with a capacitance meter for the PHCAP experiment.

Figure 8(a) shows photocapacitance transient curves for different energies as a function of illumination time at low temperature (110 K: $e^{th}_{H2} \ll e^{opt}_{H2}$). We can observe the time constant for the ionization for the $H2$ trap[22] and its dependence on the excitation wavelength.

Figure 8(b) shows the excitation photon energy dependence of the time constant of photoionization for hole emission from the $H2$ trap. The step around 1.9 eV in Fig. 8(b) is due to the band-gap excitation; the signal from the $H2$ trap comes out about 1 eV. The threshold photoionization energy of the $H2$ center for holes is evaluated theoretically[11] as follows:

$$\sigma^{opt}(E) = C[(E^{opt})^{0.5}(E-E^{opt})^{1.5}]/E^3, \tag{7}$$

where σ^{opt} is the optical cross section for the emission of a carrier, E is the excitation photon energy, C is the proportionality factor, and E^{opt} is the threshold photoexcitation energy.

The threshold photoionization energy for holes of the $H2$ trap was estimated at 0.95 ± 0.10 eV by fitting the data shown in Fig. 8(b).

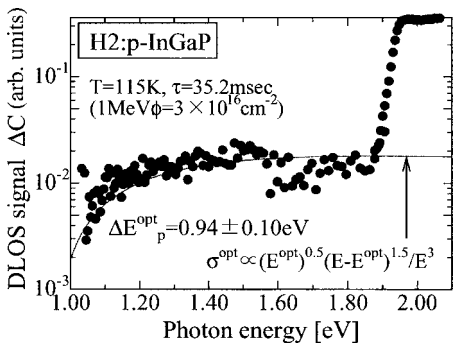

FIG. 9. DLOS signal for hole emission from the $H2$ trap. The photoionization energy is estimated at 0.94 ± 0.10 eV, in agreement with the PHCAP experiment.

2. DLOS analysis confirmed PHCAP photoionization energy

In order to confirm the PHCAP experiment, DLOS analysis[11] was carried out at 110 K, targeting the DLTS signal from the $H2$ center. In the DLOS method the photoionization spectrum is obtained by measuring the initial rate of change of transient capacitance of the $H2$ center in response to excitation by radiation of known wavelength. The photoionization energy 0.94 ± 0.10 eV was estimated by DLOS experiment as shown in Fig. 9.

From the above optical experiments, we can evaluate the Frank-Condon shift value d_{FC} (the difference between the photoionization energy 0.94 eV and the deep level $0.55-0.06$ eV) of the $H2$ center, at 0.45 eV. This corresponds to the reduction of the system energy when the trap captures a hole (see Fig. 10). This significant value indicates that this center is a strong electron-lattice relaxation-type defect.

D. Determination of configuration coordinate of the *H*2 center

The physical parameters determined in this study can be represented schematically by the configuration-coordinate diagram for the defect $H2$ as shown in Fig. 10; the parameters are summarized in Table I. This figure shows the system energy as a function of the configuration coordinate of the $H2$ center Q. This diagram of the trap can be divided into three branches.

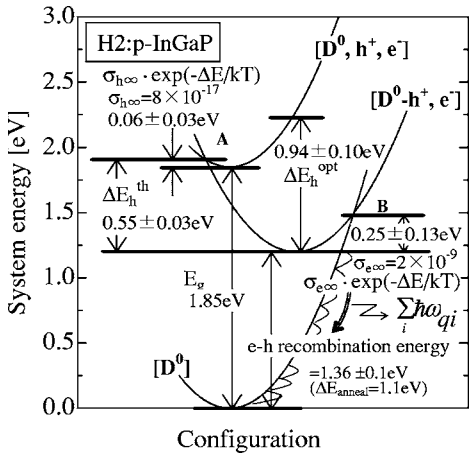

FIG. 10. Configuration-coordinate diagram of the $H2$ center. At the branch $[D_0, h^+, e^-]$, the trap is neutral with free hole (h^+) and free electron (e^-). At the branch $[D_0 - h^+, e^-]$, the hole is captured by the $H2$ center, and the electron is free. At the branch $[D_0]$, ($D_0 - h^+ - e^- \rightarrow D_0$; recombination energy), the trap is neutral again after electron-hole nonradiative recombination.

(1) The branch $[D_0, h^+, e^-]$ shows the $H2$ trap in its neutral state, with a free hole (h^+) and free electron (e^-).

(2) The branch $[D_0 - h^+, e^-]$ shows the $H2$ trap after a hole is captured and the electron is free.

(3) The branch $[D_0]$ ($D_0 - h^+ - e^- \rightarrow D_0$; recombination energy) shows the trap in its neutral state again having mediated electron-hole nonradiative recombination.

The minority-carrier capture occurs mainly at the crossing point A (Fig. 10) while the majority-carrier capture is at the point B, and hence the pair is lost by nonradiative recombination through the defect.

When the defect vibrates, the relative position of the center compared to its neighboring atoms also changes, i.e., the lattice energy E_L moves up or down in a branch. When the lattice energy is sufficiently large relative to the capture barrier ($E_L > E_{cap}$), the deep center can capture a carrier. If the defect captures a minority carrier after a majority carrier, the lattice near the center immediately vibrates violently, dissipating the e-h recombination energy, and moves directly to an equilibrium position in the system. This e-h recombination energy, is emitted into the localized $H2$ trap and assists its motion.

The defect motion should not be confused with vibrations that are not damped by phonon propagation away from the location of defect. The prefactors of the exponents in the pure and athermal annealing rates are not equal (Fig. 3), indicating that the defect motions are different from each other. The straight motion of the defect by the REDR effect can be used for its annihilation.

Thus we can discuss the e-h nonradiative recombination energy based on the REDR energy release mechanism and the configuration-coordinate diagram determined in this study. The thermal emission of a hole from the trap is the reverse of the capture with a different barrier, $E_{h,em}^{th} = 0.55$ eV, known as the activation energy. Thus, for the defect $H2$, the barrier activation energy ($E_{h,cap} = 0.06 \pm 0.03$ eV) must be subtracted from the empirical activation energy ($E_{h,em}^{th} = 0.55 \pm 0.03$ eV) for thermal emission in order to obtain the true deep-level depth ($E_T = E_{h,em}^{th} - E_{h,cap} = 0.49 \pm 0.03$ eV) appearing in the detailed balance equation

$$e_p^{th} = \sigma_p(T)\langle v_{th(p)}\rangle N_V \exp(-E_T/kT), \tag{8}$$

where $E_T = E_{h,em}^{th} - E_{h,cap}$.

The level associated with the $H2$ defect ($E_V + 0.49$ eV) is consistent with the observation that this defect plays the role of a nonradiative recombination center. As shown in Fig. 3, minority-carrier injection causes a substantial reduction in the annealing activation energy E_J as compared to the thermal annealing activation energy E_{th}, from 1.68 to 0.51 eV. The difference of 1.17 eV is the apparent energy transferred during electron capture. The energy which is released by electron trapping at the defect site is equal to the band gap of $In_xGa_{1-x}P$ at room temperature, about 1.85 eV, minus the true energy position ($E_T = E_{h,em}^{th} - E_{cap,h}$) of the defect $H2$ relative to the valence band, 0.49 eV, giving a value of 1.36 ± 0.03 eV.

Thus the energy of multiphonon emission due to the e-h recombination at the $H2$ center is evaluated as 1.36 ± 0.03 eV $[E_g - (\Delta E_{h,em}^{th} - \Delta E_{cap,h}) = 1.85 - (0.55 - 0.06)$ eV] obtained from the configuration-coordinate diagram. Under the acceptable error range, this value corresponds to the energy reduction in the annealing experiments 1.2 ± 0.2 eV between the pure-thermal and the minority-carrier injection (REDR). Therefore, the enhanced defect annealing at the $H2$ center (by electron injection) can be identified as the REDR effect and its large lattice relaxation.

Figure 11 shows that the saturated annealing rate in two different samples is directly proportional to the majority-

TABLE I. The physical parameters for the major irradiation-induced center $H2$ trap in the p-$In_xGa_{1-x}P$ cell. $\sigma_n(T) = 3 \times 10^{-12} \exp[-(0.15 \pm 0.10)/kT]$; $\sigma_p(T) = 1 \times 10^{-16} \exp[-(0.06 \pm 0.03)/kT]$.

Trap parameters	$H2$ in p-$In_xGa_{1-x}P$ (eV)
Band gap E_g	1.85
Thermal activation energy for hole $\Delta E_{h,em}^{th}$	0.55±0.03
Capture barrier height for hole $\Delta E_{h,cap}$	0.06±0.03
Optical activation energy for hole $\Delta E_{h,em}^{opt}$	0.94±0.10
Frank-Condon shift value d_{FC}	0.45±0.10
Capture barrier height for electron $\Delta E_{e\text{-}h}$ ($\Delta E_{e,cap}$)	0.15±0.10
e-h recombination energy $E_{e\text{-}h}^{rec}$	1.36±0.0

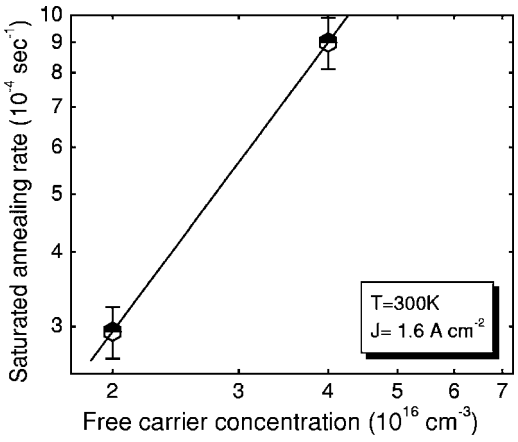

FIG. 11. Saturated recombination annealing rate of the defect $H2$ as a function of free-carrier concentration. The solid line is a linear fit to the data.

carrier (hole) concentration. This is only possible if the enhancement is proportional to the recombination rate. This is further supporting evidence that the observed minority-carrier injection annealing effect for the defects $H2$ occurs only with recombination and is independent of the defect charge state (Fig. 3).

IV. CONCLUSION

We have performed detailed studies on the stability of the defect $H2$ under various biases, and of the dependence of the annealing rates on electrical injection current densities at different temperatures by using a variety of electrical and optical techniques such as double-carrier DLTS, thermally stimulated capacitance, deep-level optical spectroscopy, and photocapacitance. The present in-depth physics-based studies fully explore the role of the major irradiation-induced center $H2$ in p-$In_xGa_{1-x}P$ as an efficient electron-hole nonrecombination center. The *e-h* recombination energy at the $H2$ center has played a role in promoting a marked recombination-enhanced defect reaction process under the minority-carrier-injection condition. A coherent picture of the $H2$ center in view of the electrical and optical experimental data analysis can be summarized as follows.

(1) Multiphonon emission during hole capture in the $H2$ center has been confirmed, i.e., the capture cross section of the electron is about three orders of magnitude larger than the hole capture cross section.

(2) A strong *e-h* recombination on the $H2$ trap has been verified by TSCAP and DCDLTS experiments.

(3) The photoionization energy (0.94 eV) estimated by DLOS confirmed the PHCAP experiments. The Frank-Condon shift value is 0.45 eV, which indicates that this center is a strong electron-lattice relaxation-type defect.

(4) A large Stokes shift is in good agreement with the proposed configuration-coordinate diagram model.

Analysis of the results based on a variety of experimental techniques reveals that the mechanism involved in the minority-carrier injection annealing of the defect is the energy release mechanism, in which enhancement is induced by the energy that is released when a minority carrier is trapped on the localized $H2$ center.

[1] A. Khan, M. Yamaguchi, J. C. Bourgoin, N. de Angelis, and T. Takamoto, Appl. Phys. Lett. **76**, 2559 (2000).
[2] A. Khan, M. Yamaguchi, T. Takamoto, N. de Angelis, and J. C. Bourgoin, J. Cryst. Growth **210**, 264 (2000).
[3] M. Yamaguchi, T. Okuda, S. J. Taylor, T. Takamoto, E. Ikeda, and H. Kurita, Appl. Phys. Lett. **70**, 1566 (1997).
[4] A. Khan, M. Yamaguchi, J. C. Bourgoin, N. de Angelis, and T. Takamoto, J. Appl. Phys. **91**, 2391 (2002).
[5] A. Khan, M. Yamaguchi, J. C. Bourgoin, and T. Takamoto, J. Appl. Phys. **89**, 4263 (2001).
[6] C. T. Sah, W. W. Chan, H. S. Fu, and J. W. Walker, Appl. Phys. Lett. **20**, 193 (1972).
[7] A. Chantre, G. Vincent, and D. Bois, Phys. Rev. B **23**, 5335 (1981).
[8] C. T. Sah, L. Forbes, L. L. Rosier, and A. F. Tasch, Jr., Solid-State Electron. **13**, 759 (1970).
[9] H. Kukimoto, C. H. Henry, and F. R. Merritt, Phys. Rev. B **7**, 2486 (1973).
[10] W. Shockley and W. T. Read, Jr., Phys. Rev. **87**, 835 (1952).
[11] G. Lucovsky, Solid State Commun. **3**, 299 (1965).
[12] D. V. Lang and L. C. Kimerling, Phys. Rev. Lett. **35**, 22 (1975).
[13] D. V. Lang, Annu. Rev. Mater. Sci. **12**, 377 (1982).
[14] D. V. Lang and C. H. Henry, Phys. Rev. Lett. **35**, 1525 (1975).
[15] J. C. Bourgoin and J. W. Corbett, Radiat. Eff. **36**, 157 (1978).
[16] L. C. Kimerling, Solid-State Electron. **21**, 1391 (1978).
[17] H. Sumi, J. Phys. C **17**, 6071 (1984).
[18] F. Seitz, Phys. Rev. **89**, 1299 (1953).
[19] L. C. Kimerling and D. V. Lang, in *Lattice Defects in Semiconductors*, IOP Conf. Proc. No. 23 (Institute of Physics, London, 1975), p. 589.
[20] J. C. Bourgoin and J. W. Corbett, Phys. Lett. **83A**, 135 (1972).
[21] J. C. Bourgoin and J. W. Corbett, in *Lattice Defects in Semiconductors*, IOP Conf. Proc. No. 23 (Ref. 19), p. 149.
[22] It should be noted that the PHCAP signals in Fig. 8 stem from hole emission σ_h^{opt} from the $H2$ center. Under this experimental condition only holes are captured, so resulting in a single PHCAP time constant. This indicates that the $H2$ hole trap is dominant.